





Article

Spectral Function of a Boson Ladder in an Artificial Gauge Field

Roberta Citro^{1,2*} , Stefania De Palo^{3,4} , Nicolas Victorin⁵, Anna Minguzzi⁵ , Edmond Orignac⁶ 

¹ Dipartimento di Fisica "E.R. Caianiello", Università degli Studi di Salerno and CNR-Spin, Via Giovanni Paolo II, 132, I-84084 Fisciano (Sa), Italy

² INFN, Sezione di Napoli, Italy

³ CNR-IOM-Democritos National Simulation Centre, UDS Via Bonomea 265, I-34136, Trieste, Italy ⁴ Dipartimento di Fisica Teorica, Università Trieste, Trieste, Italy

⁵ Univ. Grenoble-Alpes, CNRS, LPMMC, 38000 Grenoble, France

⁶ Univ Lyon, Ens de Lyon, Univ Claude Bernard, CNRS, Laboratoire de Physique, F-69342 Lyon, France

* Correspondence: rocitro@unisa.it

Abstract: We calculate the spectral function of a boson ladder in an artificial magnetic field by means of analytic approaches based on bosonization and Bogoliubov theory. We discuss the evolution of the spectral function at increasing effective magnetic flux, from the Meissner to the Vortex phase, focussing on the effects of incommensurations in momentum space. At low flux, in the Meissner phase, the spectral function displays both a gapless branch and a gapped one, while at higher flux, in the Vortex phase, the spectral function displays two gapless branches and the spectral weight is shifted at a wavevector associated to the underlying vortex spatial structure which can indicate a supersolid-like behavior. While the Bogoliubov theory, valid at weak interactions, predicts sharp delta-like features in the spectral function, at stronger interactions we find power-law broadening of the spectral functions due to quantum fluctuations as well as additional spectral weight at higher momenta due to backscattering and incommensuration effects. These features could be accessed in ultracold atom experiments using radio-frequency spectroscopy techniques.

Keywords: bosonization, Bogoliubov approximation, artificial gauge field, spectral functions

1. Introduction

In quasi one-dimensional systems, analogues of the Meissner and Vortex phase have been predicted for the bosonic two-leg ladder[1–4], the simplest system where orbital magnetic field effects are allowed. It was shown that in this model, the quantum phase transition between the Meissner and the Vortex phase is a commensurate-incommensurate transition [5–7]. Recently the advent of ultracold atomic gases, have opened a route where to realize low dimensional strongly interacting bosonic systems[8–10] where an artificial magnetic flux acting on the ladder can be simulated either using geometric phases[11], or the spin-orbit coupling[12,13]. Indeed, there is a mapping of the two-leg ladder bosonic model to a two-component spinor boson model in which the bosons in the upper leg become spin-up bosons and the bosons in the lower leg spin-down bosons. Under such mapping, the magnetic flux of the ladder becomes a spin-orbit coupling for the spinor bosons. Theoretical proposals to realize either artificial gauge fields and artificial spin orbit coupling have been put forward[14,15], and an artificial spin-orbit coupling has been achieved in a cold atoms experiment[16]. In a two-leg boson ladder the transition between a commensurate to an incommensurate phase has been characterized using equal time correlation functions[3,17–19]. However, we expect a direct

signature of the transition also in dynamical correlation functions. In one dimension, the low energy modes are collective excitations[20,21], and in the two-leg ladder, there is a separation between a total density (“charge”) and a density difference (“spin”) mode[2,4]. This is analogous to the well-known spin charge separation in electronic systems[20] and two-component boson systems[22]. Except at commensurate filling[23–26] the “charge” mode is gapless. By contrast, the “spin” mode is gapped in the Meissner phase and gapless in the Vortex phase, the transition as a function of flux being in the commensurate-incommensurate class[5,6]. Thus, the two phases are characterized by very different dynamical correlation functions. Among those correlation functions, one could for example consider the “spin-spin” dynamical structure factor. This would display a well defined gapped or gapless dispersion respectively in the Meissner and in the Vortex phase. However, such correlation function would not be sensitive to the incommensuration in the weak interchain hopping regime, although it displays incommensuration features at weak interactions and large interchain hopping[4,27]. A better indicator of incommensuration in all regimes is provided by the spectral function of the bosonic particles. In the Vortex phase, it always displays a shift in the position of the minimum of the dispersion away from $q = 0$ as a consequence of the incommensuration, whereas in the Meissner state the minimum of the dispersion remains at $q = 0$. A particular feature of the single-particle spectral function is that it is incoherent[22,28] i.e. the low energy excitation branches emerge as power law singularities instead of delta function singularities. From the experimental point of view, single-particle spectral functions are accessible via radiofrequency (RF) spectroscopy techniques [29,30]. In the present paper, we calculate the boson spectral function in the different phases of the boson ladder at incommensurate filling in order to fully characterize the transition under flux.

2. Model

In the following we use the notations and definitions of Ref. [19]. We consider a model of bosons on a two-leg ladder in the presence of an artificial U(1) gauge field[13,31]:

$$H = -t \sum_{j,\sigma} (b_{j,\sigma}^\dagger e^{i\lambda\sigma} b_{j+1,\sigma} + b_{j+1,\sigma}^\dagger e^{-i\lambda\sigma} b_{j,\sigma}) + \frac{U}{2} \sum_{j,\sigma} n_{j\sigma} (n_{j\sigma} - 1) + \frac{\Omega}{2} \sum_{j,\alpha,\beta} b_{j,\alpha}^\dagger (\sigma^x)_{\alpha\beta} b_{j,\beta}. \quad (1)$$

where $\sigma = \uparrow, \downarrow$ represents the leg index or the internal mode index[32–34], $b_{j,\sigma}$ annihilates a boson on leg σ on the j -th site, $n_{j\alpha} = b_{j\alpha}^\dagger b_{j\alpha}$, t is the hopping amplitude along the chain, Ω is the tunneling between the legs or laser induced tunneling between internal modes, λ is the flux of the effective magnetic field, U is the repulsion between bosons on the same leg. The low-energy effective theory for the Hamiltonian (1), where $\Omega \ll t$ is treated as a perturbation, is obtained by using Haldane’s bosonization.[35] By introducing the fields $\phi_\alpha(x)$ and $\Pi_\alpha(x)$ satisfying canonical commutation relations $[\phi_\alpha(x), \Pi_\beta(y)] = i\delta(x-y)$ as well as the dual $\theta_\alpha(x) = \pi \int^x dy \Pi_\alpha(y)$ of $\phi_\alpha(x)$, and after introducing the respective combinations of operators $\phi_{c,s} = \frac{1}{\sqrt{2}}(\phi_\uparrow \pm \phi_\downarrow)$ we can represent the low-energy Hamiltonian as $H = H_c + H_s$, where

$$H_c = \int \frac{dx}{2\pi} \left[u_c K_c (\pi \Pi_c)^2 + \frac{u_c}{K_c} (\partial_x \phi_c)^2 \right] \quad (2)$$

describes the total density (or charge) fluctuations for incommensurate filling when umklapp terms are irrelevant, and

$$H_s = \int \frac{dx}{2\pi} \left[u_s K_s \left(\pi \Pi_s + \frac{\lambda}{a\sqrt{2}} \right)^2 + \frac{u_s}{K_s} (\partial_x \phi_s)^2 \right] - 2\Omega A_0^2 \int dx \cos \sqrt{2}\theta_s, \quad (3)$$

describes the antisymmetric density (or spin) fluctuations. In Eq. (2) and (3), u_s and u_c are respectively the velocity of antisymmetric and total density excitations, A_0 is a non universal coefficient[20] while K_s and K_c are the corresponding Tomonaga-Luttinger (TL) exponents[36]. For two chains of hard core bosons, we have $u_c = u_s = 2t \sin(\pi\rho^0/2)$ where ρ^0 is the average number of bosons per site and

68 $K_s = K_c = 1$.

69 The phase diagram of the Hamiltonian has been determined by looking at the behavior of the chiral
70 current, *i.e.* the difference between the currents in upper and lower leg, which is defined as

$$J_s(j, \lambda) = -it \sum_{\sigma} \sigma (b_{j,\sigma}^{\dagger} e^{i\lambda\sigma} b_{j+1,\sigma} - b_{j+1,\sigma}^{\dagger} e^{-i\lambda\sigma} b_{j,\sigma}), \quad (4)$$

$$= \frac{u_s K_s}{\pi\sqrt{2}} \left(\partial_x \theta_s + \frac{\lambda}{a\sqrt{2}} \right). \quad (5)$$

71 As a function of the flux λ , the chiral current first increases linearly with λ while being in the Meissner
72 phase and above a critical value of λ it starts to decrease in the Vortex phase[2]. In this phase the rung
73 current starts to be different from zero. The phase diagram of the model can be obtained by analyzing
74 the behavior of the rung and chiral current and in Fig.1 the red-line is the phase boundary between the
75 Vortex and the Meissner phase for the non-interacting case, while the blue-line represents the phase
76 boundary in the hard-core limit[19]. The major difference with respect to the non-interacting case is
77 the persistence of the Meissner phase even for large values of the flux[17,18].

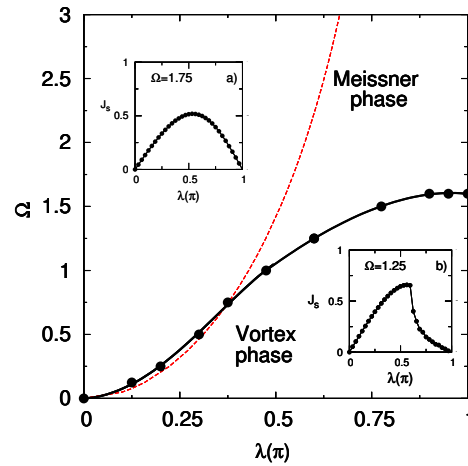


Figure 1. Phase diagram for a hard-core bosonic system on a ladder as a function of flux per plaquette λ and Ω , at the filling value $n = 1$. The black solid line that joins solid dots is the phase boundary between the Meissner and the Vortex phase, while the dashed red line is the prediction for this boundary in the non-interacting system. In the insets we show the different behavior of the spin-current $J_s(\lambda)$ for two values of interchain coupling Ω when there is the Meissner/Vortex transition and where there is not, respectively panel b) for $\Omega = 1.25$ and a) for $\Omega = 1.75$ DMRG simulation results at $L = 64$ in PBC.

78 Beyond the chiral and rung current the Meissner to Vortex phase transition can be traced out by
79 looking at the behavior of the spectral function which is more sensitive to incommensurations.

80 For the case of lattice bosons the spectral function is defined as:

$$A_{\sigma}(q, \omega) = i \sum_j \int dt \theta(t) e^{-i(qx_j - \omega t)} \left[\langle b_{j\sigma}(t) b_{0\sigma}^{\dagger}(0) \rangle - \langle b_{0\sigma}^{\dagger}(0) b_{j\sigma}(t) \rangle \right], \quad (6)$$

81 where $x_j = ja$, a being the lattice spacing, and can be experimentally accessed by, *e.g.* via
82 radiofrequency (RF) spectroscopy techniques [29,30]. In the following we will focus on the
83 positive-frequency part of the spectral function, given by the first term in Eq. (6).

84 3. Spectral function in the Meissner phase for weak interchain hopping

Within the bosonization technique the boson annihilation operator to the lowest order approximation can be represented as:

$$\psi_\sigma(x, t) = b_{j,\sigma}(\tau) / \sqrt{a} \sim A_0 \langle e^{i\frac{\theta_s}{\sqrt{2}}} \rangle e^{i\frac{\theta_c(ja,\tau)}{\sqrt{2}}}, \quad (7)$$

A_0 is a non-universal constant and σ stands for \uparrow in the upper chain and \downarrow for the lower chain. Knowing the Green's function for the field operator ψ_σ one gets the spectral function as:

$$A_\sigma(q, \omega) \sim A_0^2 |\langle e^{i\frac{\theta_s}{\sqrt{2}}} \rangle|^2 \int \frac{dxdt}{2\pi} e^{-i(qx-\omega t)} \left(\frac{\alpha^2}{(\alpha - iu_c t)^2 + x^2} \right)^{\frac{1}{8K_c}}, \quad (8)$$

where α is the theory cutoff taken equal to the lattice spacing. The result of the integral yields

$$A_\sigma(q, \omega) \sim \frac{(A_0\alpha)^2 \pi}{u_c} |\langle e^{i\frac{\theta_s(x,t)}{\sqrt{2}}} \rangle|^2 \frac{e^{\frac{2\omega}{u_c}\alpha}}{\Gamma^2\left(\frac{1}{8K_c}\right)} \left| \left(\frac{\omega^2}{u_c^2} - q^2 \right) \alpha^2 \right|^{\frac{1}{8K_c}-1} \theta(\omega) \theta\left(\frac{|\omega|}{u_c} - |q|\right), \quad (9)$$

The approximation (12) only yields the behavior of the spectral function at ω lower than the gap Δ_s in the θ_s modes. The actual correlation function can be obtained from the Form factor expansion[37–41]. The lowest contribution, from a soliton-antisoliton pair yields

$$\langle T_\tau e^{i\frac{\theta_s(x,\tau)}{\sqrt{2}}} e^{-i\frac{\theta_s(0,0)}{\sqrt{2}}} \rangle = |\langle e^{i\frac{\theta_s(x,t)}{\sqrt{2}}} \rangle|^2 + O(e^{-2\Delta_s \sqrt{(x/u_s)^2 + \tau^2}}), \quad (10)$$

85 As a result, the Fourier transform of the full Matsubara Green's function is the sum of the
 86 contribution (9) and a second contribution analytic in a strip of the upper $i\nu$ half plane of width
 87 proportional to the gap. This implies that the analytic continuation to real frequencies of this
 88 contribution is real until $\omega = 2\Delta_s$. There, a cut appears along the real frequency and the imaginary
 89 part of that contribution to the Green's function becomes nonzero. This behavior is represented
 90 schematically on Fig. 2. As the flux increases, the gap decreases linearly until it becomes zero at
 91 the commensurate-incommensurate point. At the point $K_s = 1/2$ where the Hamiltonian H_s can
 92 be fermionized, [19] the Matsubara Green's function can be calculated in terms of Ising order and
 93 disorder operators[42–46] correlation functions. If we look at the spectral function at $q = \pm 2\pi\rho_0 + \delta q$,
 94 with $\delta q \ll \rho_0$, the situation is simpler and the correlation function to be calculated is

$$A_\uparrow(2\pi\rho_0 + \delta q, \omega) \sim \int dxdt e^{-i(\delta qx - \omega t)} \left\langle e^{i\left(\frac{\theta_c}{\sqrt{2}} + \sqrt{2}\phi_c\right)(0,0)} e^{-i\left(\frac{\theta_c}{\sqrt{2}} + \sqrt{2}\phi_c\right)(x,t)} \right\rangle \langle \psi_L(0,0) \psi_L^\dagger(x,t) \rangle, \quad (11)$$

95 thus the spectral function is simply a convolution of the spectral function of a one-dimensional
 96 massive free Dirac fermion ψ_L and the spectral function of a Tomonaga-Luttinger liquid. A schematic
 97 representation of the spectral function in the Meissner phase is presented in Fig.2.

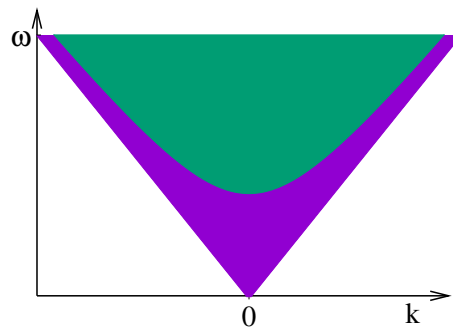


Figure 2. Schematic representation of the spectral function in the Meissner phase. The colored regions have a non-zero spectral weight. The violet region is the spectral weight coming only from the gapless charge modes, the spin modes remaining in their ground state. The green region represents the region where the gapped spin modes contribute to the spectral weight.

98 4. Spectral function in the Vortex phase for weak interchain hopping

In the vortex phase the boson field to the lowest order reads:

$$\psi_{\sigma}(x, t) = b_{j, \sigma}(\tau) / \sqrt{a} \sim A_0 e^{i\sigma q_0(\lambda) x_j} e^{i \frac{\theta_s(ja, \tau)}{\sqrt{2}}} e^{i \frac{\theta_c(ja, \tau)}{\sqrt{2}}}, \quad (12)$$

99 where $x_j = ja$, $q_0(\lambda)$ is the incommensurate wavevector of the vortex phase.

100 Thus we find the Matsubara Green's function of the bosons in the form

$$\langle T_{\tau} b_{j\sigma}(\tau) b_{0\sigma}^{\dagger}(0) \rangle = A_0^2 e^{-i\sigma q_0(\lambda) ja} \left(\frac{a^2}{(ja)^2 + (u_c \tau)^2} \right)^{\frac{1}{8K_c}} \left(\frac{a^2}{(ja)^2 + (u_s \tau)^2} \right)^{\frac{1}{8K_s^*}} \quad (13)$$

101 and the spectral function is obtained by the integral:

$$A_{\sigma}(q, \omega) \sim A_0^2 \int \frac{dx dt}{2\pi} e^{-i(qx - \omega t)} \left(\frac{\alpha}{\alpha - i(u_c t - x)} \right)^{\frac{1}{8K_c}} \left(\frac{\alpha}{\alpha - i(u_s t - x)} \right)^{\frac{1}{8K_s}} \times \left(\frac{\alpha}{\alpha - i(u_c t + x)} \right)^{\frac{1}{8K_c}} \left(\frac{\alpha}{\alpha - i(u_s t + x)} \right)^{\frac{1}{8K_s}}, \quad (14)$$

102 where $q_0(\lambda)$ is absorbed into q and $K_s \rightarrow K_s^*$. The Fourier transform of the Matsubara Green's
 103 function (13) can be calculated by the method outlined in [22,28] and after analytic continuation
 104 $iv \rightarrow \omega + i0_+$ it reads:

$$G_{\sigma}(q, \omega) = f(K_c, K_s) |\omega^2 - u_s(q + \sigma q_0(\lambda))|^{\frac{1}{8K_c} + \frac{1}{8K_s^*} - 1} e^{i\pi(1 - \frac{1}{8K_c} - \frac{1}{8K_s^*})} \Theta(\omega^2 - u_s^2(q + \sigma q_0(\lambda))^2) \times F_1 \left(\frac{1}{8K_c}, \frac{1}{8K_c} + \frac{1}{8K_s^*} - \frac{1}{2}, 1 - \frac{1}{8K_c} - \frac{1}{8K_s^*}, \frac{1}{8K_c} + \frac{1}{8K_s^*}; 1 - \frac{u_c^2}{u_s^2}, 1 - \frac{\omega^2 - u_c^2(q + \sigma q_0(\lambda))^2}{\omega^2 - u_s^2(q + \sigma q_0(\lambda))^2} \right) \quad (15)$$

105 where $f(K_c, K_s) = \left(\frac{a}{2} \right)^{\frac{1}{4K_c} + \frac{1}{4K_s^*}} \frac{\Gamma(1 - \frac{1}{8K_c} - \frac{1}{8K_s^*})}{\Gamma(\frac{1}{8K_c} + \frac{1}{8K_s^*})} u_s^{-\frac{1}{4K_c} - \frac{1}{4K_s^*} + 1}$ and the function $F_1(a, b_1, b_2, c; z_1, z_2)$ is an
 106 Appell hypergeometric function[47], which has a series representation in terms of two complex
 107 variables z_1 and z_2 when $|z_1| < 1$ and $|z_2| < 1$.

Singularities appear at $\omega_1^{\sigma}(q, \lambda) = \pm u_c(q + \sigma q_0(\lambda))$ and at $\omega_2^{\sigma}(q, \lambda) = \pm u_s(q + \sigma q_0(\lambda))$ and the power-law behavior of the spectral function near these points has been detailed in Ref. [28]. Some attention should be paid to extract the analytic continuation for points outside the radius of convergence of the Appell's function resorting to its integral representation possible when $\Re[c - a] > 0$ which in

our case is always true by construction: $c - a = 1/(8K_s^*)$. The behavior of the Green's function near the singularity points can be simplified as:

$$G_\sigma(q, \omega) \simeq |\omega^2 - \omega_1^\sigma(q, \lambda)^2|^{1/(8K_c) + 1/(4K_s^*) - 1} \quad (16)$$

$$G_\sigma(q, \omega) \simeq |\omega^2 - \omega_2^\sigma(q, \lambda)^2|^{1/(8K_s^*) + 1/(4K_c) - 1} \quad (17)$$

108 In the Vortex phase, near the commensurate-incommensurate transition the spin velocity $u_s^* \propto \sqrt{\lambda - \lambda_c}$,
 109 so we stay with the case where the charge velocity is larger than the spin one: in this case $1 - u_c^2/u_s^2 \leq 0$
 110 and $\omega_2^\sigma(q, \lambda) \leq \omega_1^\sigma(q, \lambda)$. In the Vortex phase, when the hopping between the chains is not too large,
 111 $K_s^* > 1/2$ and K_c is near unity so that the imaginary part of the Green's function, *i.e.* the spectral
 112 function $A_\sigma(q, \omega) = -\Im G_\sigma(q, \omega)/\pi$, is divergent near the two poles ω_1 and ω_2 as shown in panel *a*) of
 113 Fig.3. In order to wash out at least one of the divergencies near the two poles, small values of $K_c < 1/2$
 114 are required, signalling that density wave correlations are becoming important and eventually bringing
 115 a density-wave phase.

116 The behavior of the spin resolved spectral function $A_\sigma(q, \omega)$ for a fixed value of the applied flux is
 117 schematically shown in Fig. 3 as a function of the q and ω showing the contribution to spectral weight
 118 coming from the different singularities.

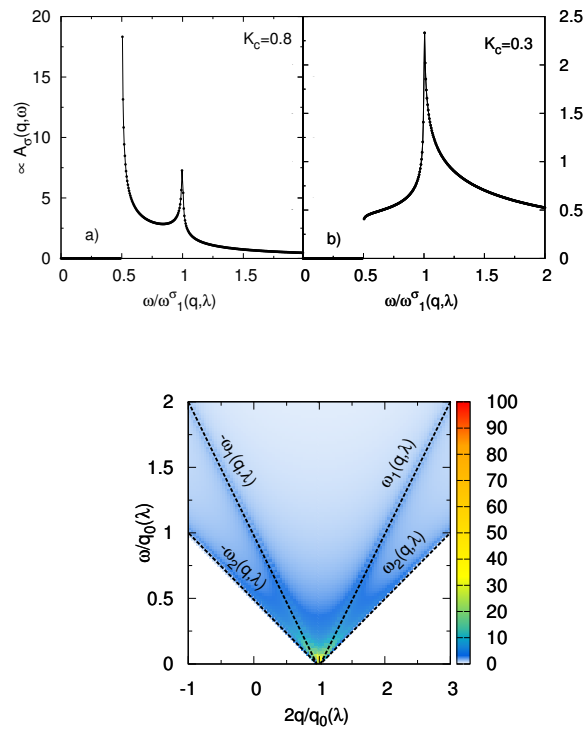


Figure 3. Spectral function $A_\sigma(q, \omega)$ as a function of $\omega/\omega_1^\sigma(q, \lambda)$ (on the top panels) for $u_s^*/u_c = 0.5$ and $K_s^* = 0.6$. In panel *a*) we show the typical situation in the Vortex phase ($K_c = 0.8$) while in panel *b*) we show the case $K_c = 0.3$. In the lower panel: $A_\sigma(q, \omega)$ as a function of ω and q for a fixed applied field λ inducing a finite $q_0(\lambda)$ for $u_s^*/u_c = 0.5$ with $K_s^* = K_c = 0.6$. Finite spectral weights are present only in the colored region. The dashed blue lines correspond to $\omega_1(q, \lambda)$ and $\omega_2(q, \lambda)$

119 5. Spectral functions in the weakly interacting regime from bosonization

120 We adopt here an alternative bosonization scheme[4], valid at weak interactions but arbitrary
 121 inter-leg tunnel coupling Ω . In this regime, one can bosonize starting from the exact single-particle
 122 excitation spectrum [4] which displays a single minimum in the Meissner phase and two minima in the
 123 Vortex phase. In the Meissner state, the result (9) is recovered, but by construction of the bosonization
 124 scheme, the contribution of gapped modes at higher energy is not accessible. In the Vortex phase, at
 125 low energy the field operators are approximated as [4]

$$\begin{aligned} b_{j\uparrow} &= u_Q \beta_{j+} e^{-iQj} + v_Q \beta_{j-} e^{iQj} \\ b_{j\downarrow} &= v_Q \beta_{j+} e^{-iQj} + u_Q \beta_{j-} e^{iQj} \end{aligned} \quad (18)$$

126 where u_Q and v_Q are the single-particle amplitudes which diagonalize the non-interacting ladder
 127 Hamiltonian, calculated at the minima $\pm Q$ of the lower branch dispersion relation, and $\beta_{j\pm} =$
 128 $\sum_q e^{-iqja} \beta_{q\pm Q}$ with β_k being the destruction operator of the lower single-particle excitation branch.
 129 Then, the field operators are bosonized as $\beta_{j\pm} = \sqrt{\bar{n}} e^{i\theta_{\pm}(x_j)}$ and the Luttinger liquid Hamiltonian
 130 takes the usual quadratic form in the symmetric, antisymmetric sectors corresponding to the operators
 131 $\theta_{s(a)} = (\theta_+ \pm \theta_-) / \sqrt{2}$. The associated Luttinger parameters are called K_s, v_s, K_a, v_a .

The Green's function, calculated *e. g.* for the upper leg $\sigma = 1/2$ reads

$$G_{\uparrow}(j, 0) = \langle b_{j\uparrow}(t) b_{0\uparrow}^{\dagger}(0) \rangle = u_Q^2 \langle \beta_{j+}(t) \beta_{0+}^{\dagger}(0) \rangle e^{-iQj} + v_Q^2 \langle \beta_{j-}(t) \beta_{0-}^{\dagger}(0) \rangle e^{iQj} \quad (19)$$

From bosonization we obtain

$$\langle \beta_{j\pm}(t) \beta_{0\pm}^{\dagger}(0) \rangle = \bar{n} \left(\frac{a^2}{(ja)^2 - (v_s t)^2} \right)^{1/(8K_s)} \left(\frac{a^2}{(ja)^2 - (v_a t)^2} \right)^{1/(8K_a)} \quad (20)$$

132 while $\langle \beta_{j\pm}(t) \beta_{0\mp}^{\dagger}(0) \rangle = 0$. This can be Fourier transformed as done in Sec.4, yielding a spectral
 133 function with two incoherent contributions at $q = \pm Q$, each with a power law singularity at the two
 134 excitation branches $\omega = v_{s,a} |q \pm Q|$. The same result is obtained in the lower leg, up to an exchange of
 135 u_Q^2 and v_Q^2 .

136 6. Spectral function in the Bogoliubov theory

137 In the previous sections we have derived the expressions for the spectral function with the
 138 bosonization technique, valid at intermediate and strong interactions. In the regime of very weak
 139 interactions and large filling of the lattice, a complementary approach is provided by the Bogoliubov
 140 theory [27]. The system is described by a two-component Bose-Einstein condensate with wavefunction
 141 $\Psi_{j\sigma}^{(0)}$ and small fluctuations on top of it. The condensate wavefunction $\Psi_{j\sigma}^{(0)}$ is obtained by solving the
 142 coupled discrete non-linear Schroedinger equations

$$\begin{aligned} \mu \Psi_{l,1}^{(0)} &= -t \Psi_{l+1,1}^{(0)} e^{i\lambda} - t \Psi_{l-1,1}^{(0)} e^{-i\lambda} \\ &\quad - (\Omega/2) \Psi_{l,2}^{(0)} + U |\Psi_{l,1}^{(0)}|^2 \Psi_{l,1}^{(0)} \\ \mu \Psi_{l,2}^{(0)} &= -t \Psi_{l+1,2}^{(0)} e^{-i\lambda} - t \Psi_{l-1,2}^{(0)} e^{i\lambda} \\ &\quad - (\Omega/2) \Psi_{l,1}^{(0)} + U |\Psi_{l,2}^{(0)}|^2 \Psi_{l,2}^{(0)}, \end{aligned} \quad (21)$$

where μ is the chemical potential. The field operator is approximated by

$$b_{j\sigma}(t) \simeq \Psi_{j\sigma}^{(0)} + \sum_v h_{vj}^{\sigma} \gamma_v - Q_{vj}^{\sigma*} \gamma_v^{\dagger}, \quad (22)$$

143 where h_{vj}^σ and Q_{vj}^σ are the Bogoliubov mode wavefunctions with energy ω_v and γ_v are the quasiparticle
 144 creation and destruction field operators, satisfying bosonic commutation relations (see [27] for the full
 145 expressions).

Using the definition (6) for the spectral function together with the mode expansion of the bosonic
 field operators (22) we obtain

$$A_\sigma(q, \omega)_\sigma = \sum_v [|\tilde{h}_{vq}^\sigma|^2 \delta(\omega - \omega_v) - |\tilde{Q}_{vq}^\sigma|^2 \delta(\omega + \omega_v)] \quad (23)$$

146 where $\tilde{h}_{vq}^\sigma = \sum_j e^{-ikaj} h_{vj}^\sigma$ and $\tilde{Q}_{vq}^\sigma = \sum_j e^{-ikaj} Q_{vj}^\sigma$.

147 The spectral function in the Bogoliubov approximation is illustrated in Fig.4. In the Meissner
 148 phase, a single branch in the spectrum is identified, corresponding to the Bogoliubov excitation mode,
 149 centered at $k = 0$. In the Vortex phase, we find two sound modes at low energy centered at $k = \pm q_0$,
 150 as well as weak branches associated to the folding of the excitation spectrum in the presence of a
 151 modulated equilibrium density profile.

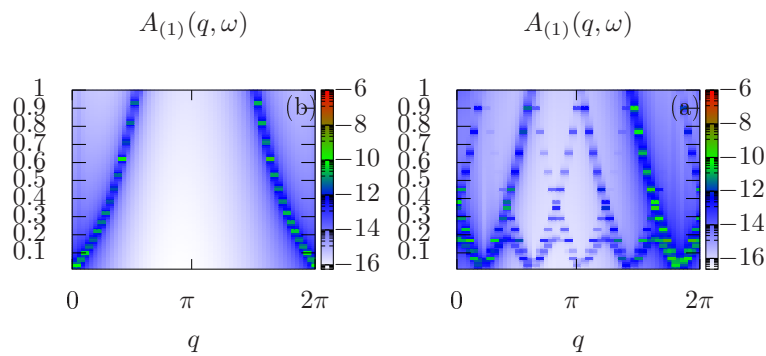


Figure 4. Spectral function $A_{\uparrow}(q, \omega)$ as a function of ω and q for a fixed applied field $\lambda = \pi/2$, in the Meissner phase (left panel, $\Omega/t = 4$) and in the Vortex phase (right panel $\Omega/t = 1.2$), for mean-field interaction parameter $UN/(N_s t) = 0.6$ and number of sites $N_s = 60$.

152 7. Conclusion

153 We have obtained the spectral functions of a two-leg boson ladder in an artificial gauge field. The
 154 bosonization approach, describing the regime of sufficiently strong interactions, predicts that in the
 155 Meissner phase, the low energy spectral weight is located near $\omega = 0, q = 0$. In the Vortex phase,
 156 it is located near $\omega = 0, \pm q_0(\lambda)$. In both cases, the spectral weight is incoherent and characterized
 157 by power law singularities at $\omega = u_c |q|$ (Meissner phase) or $\omega = u_c |q \pm q_0(\lambda)|$ (Vortex phase) with
 158 known exponents, and a specific incommensuration effect due to the shift of the spectral weight for
 159 $q \simeq q_0(\lambda)/2$. In the Meissner phase, the gap in the antisymmetric density fluctuations translates as a
 160 power law singularity of the spectral function at frequency $\omega > 2\Delta_s$. The Bogoliubov approximation,
 161 valid at weak interactions predicts delta-like spectral function, still keeping the main features: a
 162 single gapless excitation branch and a gapped one in the Meissner phase and two gapless excitation
 163 branches displaying incommensuration effects in the Vortex phase. The Bogoliubov theory misses the
 164 backscattering contributions to the spectral function, consistently with the bosonization predictions
 165 that their spectral weight is very small at weak interactions.

166 The present work could be extended in different directions. Exactly at the
 167 commensurate-incommensurate transition, the antisymmetric excitations are described by a
 168 gapless theory[48] with dynamical exponent $z = 2$. The finite temperature correlation function has a
 169 known scaling form[49,50], and the spectral function at the commensurate-incommensurate transition
 170 can be obtained by convolution of that correlation function with the one of the charge modes. Such
 171 calculation is left for future work. Another possible extension is to consider the interleg interaction.
 172 Previous work has shown[36,51] that it splits the commensurate incommensurate transition point

173 into an Ising transition point, a disorder point and a Berezinskii-Kosterlitz-Thouless (BKT) transition
 174 point. An intermediate atomic density wave exists between the Ising and the BKT point, and it
 175 develops incommensuration at the disorder point. The atomic density wave could be characterized
 176 using the spectral functions as done in the present manuscript, both in its commensurate and in its
 177 incommensurate regime. A final possible extension is to consider the spectral functions in the presence
 178 of the second incommensuration[19,52] at $\lambda = \pi n$.

179 **Acknowledgments:** AM and NV acknowledge funding from ANR SuperRing project (Grant No.
 180 ANR-15-CE30-0012).

181 References

- 182 1. Kardar, M. Josephson-junction ladders and quantum fluctuations. *Phys. Rev. B* **1986**, *33*, 3125.
- 183 2. Orignac, E.; Giamarchi, T. Meissner effect in a bosonic ladder. *Phys. Rev. B* **2001**, *64*, 144515.
- 184 3. Cha, M.C.; Shin, J.G. Two peaks in the momentum distribution of bosons in a weakly frustrated two-leg
 185 optical ladder. *Phys. Rev. A* **2011**, *83*, 055602.
- 186 4. Tokuno, A.; Georges, A. Ground States of a Bose-Hubbard Ladder in an Artificial Magnetic Field:
 187 Field-Theoretical Approach. *New J. Phys.* **2014**, *16*, 073005. doi:10.1088/1367-2630/16/7/073005.
- 188 5. Japaridze, G.I.; Nersisyan, A.A. *JETP Lett.* **1978**, *27*, 334.
- 189 6. Pokrovsky, V.L.; Talapov, A.L. *Phys. Rev. Lett.* **1979**, *42*, 65.
- 190 7. Schulz, H.J. *Phys. Rev. B* **1980**, *22*, 5274.
- 191 8. Jaksch, D.; Zoller, P. The cold atom Hubbard toolbox. *Ann. Phys. (N. Y.)* **2005**, *315*, 52. cond-mat/0410614.
- 192 9. Lewenstein, M.; Sanpera, A.; Ahufinger, V.; Damski, B.; Sen De, A.; Sen, U. Ultracold atomic gases in
 193 optical lattices: mimicking condensed matter physics and beyond. *Ann. Phys. (N. Y.)* **2007**, *56*, 243.
 194 cond-mat/0606771.
- 195 10. Bloch, I.; Dalibard, J.; Zwirger, W. Many-body physics with ultracold gases. *Rev. Mod. Phys.* **2008**, *80*, 885.
 196 doi:10.1103/RevModPhys.80.885.
- 197 11. Dalibard, J.; Gerbier, F.; Juzeliūnas, G.; Öhberg, P. Colloquium: Artificial gauge potentials for neutral atoms.
 198 *Rev. Mod. Phys.* **2011**, *83*, 1523.
- 199 12. Zhang, S.; Cole, W.S.; Paramakanti, A.; Trivedi, N. Spin-Orbit Coupling In Optical Lattices. In *Annual*
 200 *Review of Cold Atoms and Molecules*; Madison, K.W.; Bongs, K.; Carr, L.D.; Rey, A.M.; Zhai, H., Eds.; World
 201 Scientific: Singapore, 2015; Vol. 3, chapter 3, p. 135. arXiv:1411.2297, doi:10.1142/9789814667746_0003.
- 202 13. Barbarino, S.; Taddia, L.; Rossini, D.; Mazza, L.; Fazio, R. Synthetic gauge fields in synthetic dimensions:
 203 interactions and chiral edge modes. *New J. Phys.* **2016**, *18*, 035010.
- 204 14. Osterloh, K.; Baig, M.; Santos, L.; Zoller, P.; Lewenstein, M. Cold Atoms in Non-Abelian Gauge
 205 Potentials: From the Hofstadter "Moth" to Lattice Gauge Theory. *Phys. Rev. Lett.* **2005**, *95*, 010403.
 206 doi:10.1103/PhysRevLett.95.010403.
- 207 15. Ruseckas, J.; Juzeliūnas, G.; Öhberg, P.; Fleischhauer, M. Non-Abelian Gauge Potentials for Ultracold
 208 Atoms with Degenerate Dark States. *Phys. Rev. Lett.* **2005**, *95*, 010404. doi:10.1103/PhysRevLett.95.010404.
- 209 16. Lin, Y.; Jimenez-Garcia, K.; Spielman, I.B. Spin-orbit-coupled Bose-Einstein condensates. *Nature (London)*
 210 **2011**, *471*, 83.
- 211 17. Piraud, M.; Cai, Z.; McCulloch, I.P.; Schollwöck, U. Quantum magnetism of bosons with synthetic gauge
 212 fields in one-dimensional optical lattices: a Density Matrix Renormalization Group study. *Phys. Rev. A*
 213 **2014**, *89*, 063618.
- 214 18. Piraud, M.; Heidrich-Meisner, F.; McCulloch, I.P.; Greschner, S.; Vekua, T.; Schollwöck, U. Vortex and
 215 Meissner phases of strongly interacting bosons on a two-leg ladder. *Phys. Rev. B* **2015**, *91*, 140406.
 216 doi:10.1103/PhysRevB.91.140406.
- 217 19. Orignac, E.; Citro, R.; Di Dio, M.; De Palo, S.; Chiofalo, M.L. Incommensurate phases of a bosonic two-leg
 218 ladder under a flux. *New J. Phys.* **2016**, *18*, 055017. doi:10.1088/1367-2630/18/5/055017.
- 219 20. Giamarchi, T. *Quantum Physics in One Dimension*; Oxford University Press: Oxford, 2004.
- 220 21. Cazalilla, M.A.; Citro, R.; Giamarchi, T.; Orignac, E.; Rigol, M. One dimensional Bosons: From Condensed
 221 Matter Systems to Ultracold Gases. *Rev. Mod. Phys.* **2011**, *83*, 1405.

- 222 22. Kleine, A.; Kollath, C.; McCulloch, I.; Giamarchi, T.; Schollwoeck, U. Spin-charge separation in
223 two-component Bose gases. *Phys. Rev. A* **2008**, *77*, 013607. arXiv:0706.0709.
- 224 23. Dhar, A.; Maji, M.; Mishra, T.; Pai, R.V.; Mukerjee, S.; Paramakanti, A. Bose-Hubbard model in a strong
225 effective magnetic field: Emergence of a chiral Mott insulator ground state. *Phys. Rev. A* **2012**, *85*, 041602.
226 doi:10.1103/PhysRevA.85.041602.
- 227 24. Dhar, A.; Mishra, T.; Maji, M.; Pai, R.V.; Mukerjee, S.; Paramakanti, A. Chiral Mott insulator with
228 staggered loop currents in the fully frustrated Bose-Hubbard model. *Phys. Rev. B* **2013**, *87*, 174501.
229 doi:10.1103/PhysRevB.87.174501.
- 230 25. Petrescu, A.; Le Hur, K. Bosonic Mott Insulator with Meissner Currents. *Phys. Rev. Lett.* **2013**, *111*, 150601.
231 doi:10.1103/PhysRevLett.111.150601.
- 232 26. Petrescu, A.; Le Hur, K. Chiral Mott insulators, Meissner effect, and Laughlin states in quantum ladders.
233 *Phys. Rev. B* **2015**, *91*, 054520. doi:10.1103/PhysRevB.91.054520.
- 234 27. Victorin, N.; Pedri, P.; Minguzzi, A. Excitation spectrum and supersolidity of a two-leg bosonic ring ladder.
235 *Phys. Rev. A* **2020**. to appear; arXiv:1910.06410.
- 236 28. Iucci, A.; Fiete, G.A.; Giamarchi, T. Fourier transform of the $2k_F$ Luttinger liquid density correlation
237 function with different spin and charge velocities. *Phys. Rev. B* **2007**, *75*, 205116, [arXiv:cond-mat/0702274].
238 doi:10.1103/PhysRevB.75.205116.
- 239 29. Dao, T.L.; Georges, A.; Dalibard, J.; Salomon, C.; Carusotto, I. Measuring the One-Particle Excitations
240 of Ultracold Fermionic Atoms by Stimulated Raman Spectroscopy. *Phys. Rev. Lett.* **2007**, *98*, 240402.
241 doi:10.1103/PhysRevLett.98.240402.
- 242 30. Stewart, J.T.; Gaebler, J.P.; Jin, D.S. Using photoemission spectroscopy to probe a strongly interacting Fermi
243 gas. *Nature* **2008**, *454*, 744. doi:10.1038/nature07172.
- 244 31. Strinati, M.C.; Cornfeld, E.; Rossini, D.; Barbarino, S.; Dalmonte, M.; Fazio, R.; Sela, E.; Mazza, L.
245 Laughlin-like states in bosonic and fermionic atomic synthetic ladders. *Phys. Rev. X* **2017**, *7*, 021033.
- 246 32. Celi, A.; Massignan, P.; Ruseckas, J.; Goldman, N.; Spielman, I.B.; Juzeliūnas, G.; Lewenstein,
247 M. Synthetic Gauge Fields in Synthetic Dimensions. *Phys. Rev. Lett.* **2014**, *112*, 043001.
248 doi:10.1103/PhysRevLett.112.043001.
- 249 33. Saito, T.Y.; Furukawa, S. Devil's staircases in synthetic dimensions and gauge fields. *Phys. Rev. A* **2017**,
250 *95*, 043613.
- 251 34. Livi, L.F.; Cappellini, G.; Diem, M.; Franchi, L.; Clivati, C.; Frittelli, M.; Levi, F.; Calonico, D.; Catani, J.;
252 Inguscio, M.; Fallani, L. Synthetic Dimensions and Spin-Orbit Coupling with an Optical Clock Transition.
253 *Phys. Rev. Lett.* **2016**, *117*, 220401. doi:10.1103/PhysRevLett.117.220401.
- 254 35. Haldane, F.D.M. *Phys. Rev. Lett.* **1981**, *47*, 1840.
- 255 36. Citro, R.; Palo, S.D.; Dio, M.D.; Orignac, E. Quantum phase transitions of a two-leg bosonic ladder in an
256 artificial gauge field. *Phys. Rev. B* **2018**, *97*, 174523, [arXiv:1802.04997].
- 257 37. Karowski, M.; Wiesz, P. Exact form factors in (1+1)Dimensional Field theoretic models with soliton
258 behavior. *Nucl. Phys. B* **1978**, *139*, 455.
- 259 38. Smirnov, F.A. *Form Factors in Completely Integrable Models of Quantum Field Theory*; World Scientific:
260 Singapore, 1992.
- 261 39. Babujian, H.; Fring, A.; Karowski, M.; Zapletal, A. Exact Form Factors in Integrable Quantum Field
262 Theories: the Sine-Gordon Model. *Nucl. Phys. B* **1999**, *538*, 535. hep-th/9805185.
- 263 40. Babujian, H.; Karowski, M. Exact form factors in integrable quantum field theories: the sine-Gordon model
264 (II). *Nucl. Phys. B* **2002**, *620*, 407. hep-th/0105178.
- 265 41. Essler, F.H.; Konik, R.M. Applications of Massive Integrable Quantum Field Theories to Problems in
266 Condensed Matter Physics. cond-mat/0412421.
- 267 42. José, J.V.; Kadanoff, L.P.; Kirkpatrick, S.; Nelson, D.R. *Phys. Rev. B* **1977**, *16*, 1217.
- 268 43. Zuber, J.B.; Itzykson, C. *Phys. Rev. D* **1977**, *15*, 2875.
- 269 44. Schroer, B.; Truong, T.T. The order/disorder quantum field operators associated with the two-dimensional
270 Ising model in the continuum limit. *Nucl. Phys. B* **1978**, *144*, 80.
- 271 45. Ogilvie, M. *Ann. Phys. (N. Y.)* **1981**, *136*, 273.
- 272 46. Boyanovsky, D. *Phys. Rev. B* **1989**, *39*, 6744.
- 273 47. Olver, F.; Lozier, D.; Boisvert, R.; Clark, C., Eds. *NIST handbook of mathematical functions*; Cambridge
274 University Press: Cambridge, UK, 2010.

- 275 48. Sachdev, S.; Senthil, T.; Shankar, R. *Phys. Rev. B* **1994**, *50*, 258.
- 276 49. Barthel, T.; Schollwöck, U.; Sachdev, S. Scaling of the thermal spectral function for quantum critical bosons
277 in one dimension. arXiv:1212.3570, 2012.
- 278 50. Blosser, D.; Bhartiya, V.K.; Voneshen, D.J.; Zheludev, A. $S_z=2$ Quantum Critical Dynamics in a Spin
279 Ladder. *Phys. Rev. Lett.* **2018**, *121*, 247201. doi:10.1103/PhysRevLett.121.247201.
- 280 51. Orignac, E.; Citro, R.; Di Dio, M.; De Palo, S. Vortex lattice melting in a boson-ladder in artificial gauge f
281 ield. *Phys. Rev. B* **2017**, *96*, 014518. arXiv:1703.07742, doi:10.1103/PhysRevB.96.014518.
- 282 52. Di Dio, M.; De Palo, S.; Orignac, E.; Citro, R.; Chiofalo, M.L. Persisting Meissner state and incommensurate
283 phases of hard-core boson ladders in a flux. *Phys. Rev. B* **2015**, *92*, 060506. doi:10.1103/PhysRevB.92.060506.